# A $[Cu_2O]^{2+}$ core in Cu-ZSM-5, the active site in the oxidation of methane to methanol

Julia S. Woertink[a], Pieter J. Smeets[a,b], Marijke H. Groothaert[b], Michael A. Vance[a], Bert F. Sels[b], Robert A. Schoonheydt[b,1], and Edward I. Solomon[a,1]

[a]Department of Chemistry, Stanford University, Stanford, CA 94305; and [b]Center for Surface Chemistry and Catalysis, K.U.Leuven, Kasteelpark Arenberg 23, B-3001 Leuven, Belgium

Contributed by Edward I. Solomon, September 12, 2009 (sent for review August 18, 2009)

**Driven by the depletion of crude oil, the direct oxidation of methane to methanol has been of considerable interest. Promising low-temperature activity of an oxygen-activated zeolite, Cu-ZSM-5, has recently been reported in this selective oxidation and the active site in this reaction correlates with an absorption feature at 22,700 $cm^{-1}$. In the present study, this absorption band is used to selectively resonance enhance Raman vibrations of this active site. $^{18}O_2$ labeling experiments allow definitive assignment of the observed vibrations and exclude all previously characterized copper-oxygen species for the active site. In combination with DFT and normal coordinate analysis calculations, the oxygen activated Cu core is uniquely defined as a bent mono-($\mu$-oxo)dicupric site. Spectroscopically validated electronic structure calculations show polarization of the low-lying singly-occupied molecular orbital of the $[Cu_2O]^{2+}$ core, which is directed into the zeolite channel, upon approach of $CH_4$. This induces significant oxyl character into the bridging O atom leading to a low transition state energy consistent with experiment and explains why the bent mono-($\mu$-oxo)dicupric core is highly activated for H atom abstraction from $CH_4$. The oxygen intermediate of Cu-ZSM-5 is now the most well defined species active in the methane monooxygenase reaction.**

density functional theory | dicopper(II)-oxo | oxygen activation | resonance Raman spectroscopy | zeolite

Methane, the major component of natural gas, is highly abundant and its selective oxidation to a liquid form such as methanol would help harness its potential as a petroleum alternative for fuels and in the petrochemical industry. Currently, industrial methanol production from methane is accomplished by the steam reforming of methane into syngas, a mixture of $H_2$ and CO, followed by methanol synthesis. These processes require high temperatures and pressures and as a result, alternatives such as the selective direct oxidation of methane to methanol are of considerable interest. However, methane has the strongest C—H bond of any hydrocarbon (104 kcal/mol), thus its selective oxidation to methanol without further oxidation is extremely challenging.

In nature, the methane monooxygenase (MMO) enzymes accomplish the direct conversion of methane into methanol at ambient temperatures at iron- or copper-oxygen active sites (1–3). Researchers have attempted to mimic MMO's activity synthetically by creating oxygen-activated iron and copper catalysts (4). Recently, an $O_2$-activated zeolite Cu-ZSM-5 has been shown to convert methane to methanol at low temperatures (100 °C) with selectivity >98% (5). Reactivity only occurs at a small fraction of the total copper sites in the zeolite (5). Researchers have attempted to determine the identity of the active copper-oxygen core, although the challenge of distinguishing it from spectator sites has not been overcome and no consensus has been reached as to its structure (6–8). The oxygen-activated site of Cu-ZSM-5 was correlated to an absorption feature at 22,700 $cm^{-1}$, a spectroscopic handle unique to the reactive core (6). An absorption feature at this energy, however, is not sufficient to unambiguously define the nature of the active site. In the present study, the Raman vibrations corresponding only to the active site are selectively resonance enhanced, providing detailed experimental insight. The same active site can be generated with $N_2O$ and is shown to be capable of selective methane oxidation. The resonance Raman (rR) and absorption data are coupled to normal coordinate (NCA) and density functional theory (DFT) calculations to define the geometric and electronic structure of the active site of oxygen-activated Cu-ZSM-5 and the nature of its activation for H atom abstraction.

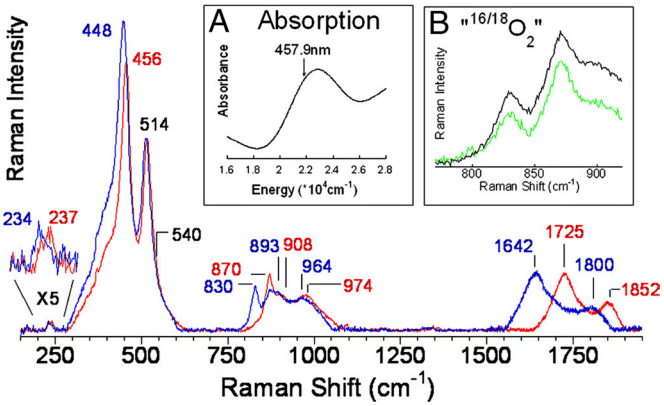


**Fig. 1.** rR spectra ($\lambda_{ex}$ = 457.9 nm) of Cu-ZSM-5 + $^{16}O_2$ (red), $^{18}O_2$ (blue). *Inset A*: Absorption spectrum of oxygen activated Cu-ZSM-5. *Inset B*: "$^{16,18}O_2$" (green), and 1:1 normalized sum of $^{16}O_2$ and $^{18}O_2$ (black).

## Results and Discussion

**Spectroscopic Characterization of the Active Core in Oxygen-Activated Cu-ZSM-5.** Tuning a laser into the characteristic absorption feature (Fig. 1 *Inset A*) of the oxygen-activated Cu-ZSM-5 active site leads to resonance enhancement of Raman vibrations associated only with this chromophore and therefore the active site for methanol synthesis (Fig. 1). The rR spectra show multiple vibrations that profile the absorption band (Fig. 2*A*)*, confirming that these vibrations are in-resonance with this electronic transition. These vibrations gain intensity with increasing Cu/Al ratio (as does the 22,700 $cm^{-1}$ absorption feature) (Fig. 2*B*) and are not observed

Author contributions: B.F.S., R.A.S., and E.I.S. designed research; J.S.W., P.J.S., M.H.G., and M.A.V. performed research; J.S.W. and P.J.S. analyzed data; and J.S.W., P.J.S., and E.I.S. wrote the paper.

The authors declare no conflict of interest.

See Commentary on page 18877.

[1]To whom correspondence may be addressed. E-mail: robert.schoonheydt@biw.kuleuven.be or edward.solomon@stanford.edu.

*Peak fits of the rR spectra in Fig. 1 are given in Fig. S1.

This article contains supporting information online at www.pnas.org/cgi/content/full/0910461106/DCSupplemental.

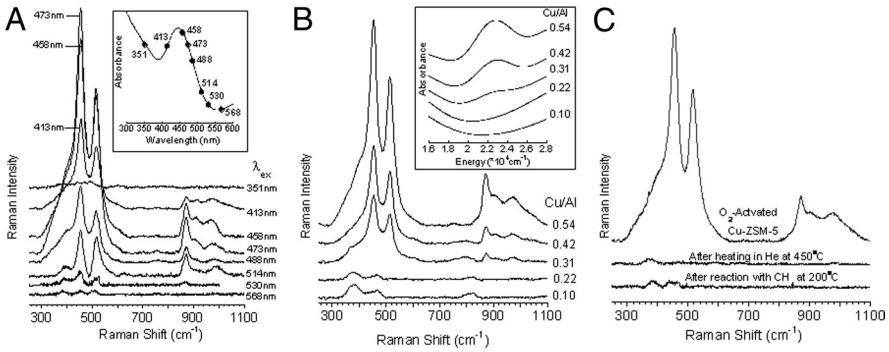


**Fig. 2.** rR spectra of $O_2$-activated Cu-ZSM-5. (*A*) rR spectra of $O_2$-activated Cu-ZSM-5 (Cu/Al = 0.54) collected at eight $\lambda_{ex}$s from 351 nm to 568 nm with corresponding absorption spectrum *Inset*. (*B*) rR spectra ($\lambda_{ex}$ = 457.9 nm) of $O_2$-activated Cu-ZSM-5 with varying Cu/Al ratios from 0.10 to 0.54 with corresponding absorption spectra *Inset*. (*C*) rR spectra ($\lambda_{ex}$ = 457.9 nm) of Cu-ZSM-5 (Cu/Al = 0.54) pretreated in $O_2$ at 450 °C, recorded before and after heating in He at 450 °C and after reaction with $CH_4$ at 200 °C.

after the site reacts with $CH_4$ (at 200 °C) or is heated in He >350 °C (Fig. 2*C*) [both lead to loss of the 22,700 $cm^{-1}$ band (9)], confirming that the vibrations observed are from the active site. A number of these resonance enhanced vibrations are sensitive to isotope perturbation when the active site is generated with $^{18}O_2$ (Fig. 1 blue). These isotope-sensitive vibrations involve the active oxygen species, as the reaction of the $^{18}O_2$-generated active site with $CH_4$ results in $CH_3{}^{18}OH$ formation (5). The most intense isotope-sensitive vibration is at 456 $cm^{-1}$ ($\Delta(^{18}O_2)$ = 8 $cm^{-1}$) and additional isotope-sensitive vibrations are at 237 $cm^{-1}$ ($\Delta(^{18}O_2)$ = 3 $cm^{-1}$), 870 $cm^{-1}$ ($\Delta(^{18}O_2)$ = 40 $cm^{-1}$), 1,725 $cm^{-1}$ ($\Delta(^{18}O_2)$ = 83 $cm^{-1}$), and 1,852 $cm^{-1}$ ($\Delta(^{18}O_2)$ = 52 $cm^{-1}$) (Fig. 1). A broad resonance enhanced feature is observed at 974 $cm^{-1}$ ($\Delta(^{18}O_2)$ = 10 $cm^{-1}$) corresponding to the combination band of the 514 $cm^{-1}$ and 456 $cm^{-1}$ vibrations based on energy and isotope shift. The second member of a progression of the 456 $cm^{-1}$ vibration is observed at 908 $cm^{-1}$ ($\Delta(^{18}O_2)$ = 15 $cm^{-1}$). An intense isotope-insensitive feature is also observed at 514 $cm^{-1}$ with a shoulder near 540 $cm^{-1}$.

These data uniquely define the geometric and electronic structure of the oxygen-activated Cu-ZSM-5 active site. In past work, the oxygen intermediate of Cu-ZSM-5 was assigned as a bis($\mu$-oxo)dicopper(III) core based on the observation of an absorption feature at 22,700 $cm^{-1}$ and a Cu—Cu distance of ≈2.9 Å from EXAFS studies of $O_2$ activated Cu-ZSM-5 (6). However, this activated Cu core accounts for only a small fraction of the total Cu content in Cu-ZSM-5 (≈5%) (5, 9), making it impossible to distinguish its contribution to the EXAFS data from that of the abundantly present spectator Cu sites. Thus, EXAFS cannot provide structural information for this core. A bis($\mu$-oxo)dicopper(III) complex is characterized by an intense isotope-sensitive stretch ≈600 $cm^{-1}$ in its rR spectrum (10, 11). The absence of such a feature in the rR spectrum of the oxygen intermediate of Cu-ZSM-5 excludes the assignment of the active site as a bis($\mu$-oxo)dicopper(III) complex. Further, the observed stretches are inconsistent with the assignment of the site structure as a $\mu$-($\eta^2$:$\eta^2$) peroxo dicopper(II) ($\nu$Cu—Cu~270 $cm^{-1}$, $\nu$O—O~750 $cm^{-1}$) (12) or a Cu(II)-superoxo ($\nu$O—O~1,050–1,100 $cm^{-1}$) species (13, 14) (Table 1). The 870 $cm^{-1}$ vibration does occur at a reasonable energy for an O—O stretch of an $\eta^1$-hydroperoxo copper(II) or a $\mu$-1,2-peroxo or hydroperoxo dicopper(II) species (15–17) (Table 1). To evaluate these possibilities, the Cu-ZSM-5 oxygen intermediate was formed with mixed isotope $O_2$ ("$^{16,18}O_2$"), a statistical mixture of $^{16}O_2$:$^{16/18}O_2$:$^{18}O_2$ (1:2:1 ratio). If the 870 $cm^{-1}$ vibration is an O—O stretch, vibrations would be observed at 830, ≈845 and 870 $cm^{-1}$ with a 1:2:1 intensity pattern, with the feature at ≈845 $cm^{-1}$ representing the $^{16}O^{18}O$ and $^{18}O^{16}O$ stretches (18, 19). Fig. 1 B *Inset* (green) shows the rR spectrum of the active species prepared with "$^{16,18}O_2$," which overlays a 1:1 normalized sum of the pure $^{16}O_2$ (red) and $^{18}O_2$ (blue) spectra (black in Fig. 1, *Inset* B). The absence of an intermediate stretch ≈845 $cm^{-1}$ eliminates the possibility that the site is a $\mu$-1,2-peroxo or hydroperoxo dicopper(II) species. Thus, all presently known copper-oxygen active site structures for the oxygen intermediate of Cu-ZSM-5 are excluded by the rR data (Table 1).

In fact, the most intense isotope sensitive feature is the 456 $cm^{-1}$ ($\Delta(^{18}O_2)$ = 8 $cm^{-1}$) stretch; the 870 $cm^{-1}$ ($\Delta(^{18}O_2)$ = 40 $cm^{-1}$) vibration has relatively low intensity but its second quantum (based on isotope shift) is observed at 1,725 $cm^{-1}$ ($\Delta(^{18}O_2)$ = 83 $cm^{-1}$) with 6 times higher intensity than the fundamental. This intensity pattern has been observed in $\mu$-oxo-diferric complexes (20). The observed high intensity of the 456 $cm^{-1}$ isotope sensitive vibration in Fig. 1 supports its assignment as the symmetric stretch of an oxo group bridging two Cu centers (21). The weak 870 $cm^{-1}$ vibration is then assigned as an antisymmetric metal-oxo stretch ($\nu_{as}$), which should not be enhanced in the rR spectrum, while its second quantum ($2\nu_{as}$) is symmetric and consequently would have higher rR intensity than the fundamental, as observed for the 1,725 $cm^{-1}$ vibration.[†] The energy of the second quantum of the $\nu_{as}$ for $^{16}O_2$-activated Cu-ZSM-5 is expected to be at twice the energy of the fundamental (1,740 $cm^{-1}$) but is instead observed at 1,725 $cm^{-1}$. Further, both the energy splitting and the intensity of the 1,725 $cm^{-1}$ peak relative to the nearby 1,852 $cm^{-1}$ peak change upon $^{18}O_2$-isotopic labeling. This is consistent with a Fermi resonance between two $^{18}O$-isotope sensitive features i.e., the fourth quantum of $\nu_s$ ($4\nu_s$, predicted at 1,824 $cm^{-1}$) and $2\nu_{as}$ (Fig. S2). The

**Table 1. Spectroscopically characterized mononuclear and binuclear Cu/$O_2$ species**

| Cu/$O_2$ species | rR vibrations ($\Delta^{18}O_2$) /$cm^{-1}$ |
|---|---|
| *$O_2$ activated Cu-ZSM-5* | *456 (8)*<br>*870 (40)* |
| bis(μ-oxo) dicopper(III) 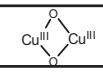 | $\nu_{Cu-O}$=606 (23) |
| μ-($\eta^2$:$\eta^2$) peroxo dicopper(II) 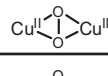 | $\nu_{Cu-Cu}$=284 (0)<br>$\nu_{O-O}$=763 (40) |
| $\eta^1$-superoxo copper(II) 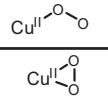 | $\nu_{Cu-O}$=472 (20)<br>$\nu_{O-O}$=1121 (63) |
| $\eta^2$-superoxo copper(II) 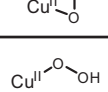 | $\nu_{Cu-O}$=554 (20)<br>$\nu_{O-O}$=1043 (59) |
| $\eta^1$-hydroperoxo copper(II) 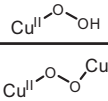 | $\nu_{Cu-O}$=624 (17)<br>$\nu_{O-O}$=843 (44) |
| trans-μ-1,2-peroxo dicopper(II) 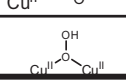 | $\nu_{Cu-O}$=561 (26)<br>$\nu_{O-O}$=832 (44) |
| μ-1,1-hydroperoxo dicopper(II)  | $\nu_{Cu-O}$=322 (10)<br>$\nu_{O-O}$=892 (52) |

[†]Constraints imposed by the zeolite lattice distort the bent Cu—O—Cu core, lowering its symmetry and enabling $\nu_{as}$ to become weakly Raman allowed and thus observable, but with low resonance intensity.

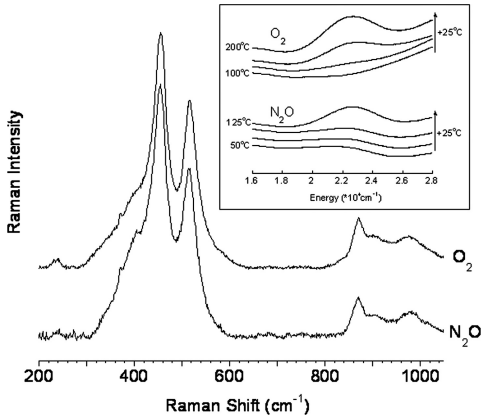


**Fig. 3.** rR spectra ($\lambda_{ex}$ = 457.9 nm) of Cu-ZSM-5 (Cu/Al = 0.54) activated in $O_2$ (*Upper*) or $N_2O$ (*Lower*). *Inset* Diffuse reflectance UV-vis spectra recorded at room temperature after treatment of Cu-ZSM-5 with $O_2$ (*Upper*) or $N_2O$ (*Lower*) in the temperature range of 100 °C-200 °C and 50–125 °C respectively. The arrows on *Inset* represent the increasing temperature of the $O_2$ and $N_2O$ treatment (temperature difference between two spectra is 25 °C).

presence of both strong symmetric and weak antisymmetric stretches leads to the assignment of the Cu-ZSM-5 active site as a bent Cu—O—Cu core.

The presence of such a core in Cu-ZSM-5 has been proposed as an intermediate during dehydration based on EXAFS data (22), but as no absorption feature is observed under these reaction conditions (9) formation of the bent Cu—O—Cu core defined here can be excluded for this process. Computational studies on Cu-ZSM-5 have surveyed the possible stabilization of several binuclear Cu sites in Cu-ZSM-5, including Cu—$O_2$—Cu and Cu—O—Cu cores (7, 23), but without spectroscopic data to discriminate among them, no assignment of the active site structure could be made. The presence of a bent Cu—O—Cu core in synthetic model complexes has been proposed (24–26), but to date, no such complex has been unambiguously defined. As a result, the data reported in the present study are the first to definitively characterize a mono-oxygen bridged binuclear Cu site in any system. Activation of Cu-ZSM-5 by $N_2O$ instead of $O_2$ also results in the formation of an absorption feature at 22,700 $cm^{-1}$. Starting from a dehydrated Cu-ZSM-5 (450 °C in He), this absorption feature is observed at lower temperatures (100 °C) than for the $O_2$ activation reaction (175 °C) (Fig. 3, *Inset*). rR spectra were collected on the $N_2O$ activated core of Cu-ZSM-5 and compared with the rR vibrations observed for the $O_2$ activated core in Fig. 3. Identical rR features are observed after both treatments, confirming that activation of Cu-ZSM-5 by either $O_2$ or $N_2O$ results in formation of the same active site (Fig. 3). This $N_2O$-generated active core is also capable of low-temperature selective oxidation of $CH_4$ to $CH_3OH$ to an extent comparable to the $O_2$ activated Cu-ZSM-5 site (14 ± 2 $\mu$mol per gram of Cu-ZSM-5).

**Geometric and Electronic Structure of the $Cu_2O$ Core in Cu-ZSM-5.** Normal coordinate analysis (NCA) was used to correlate the observed rR symmetric ($\nu_s$) and antisymmetric ($\nu_{as}$) vibrations and their isotope shifts to the bending angle for a $Cu_2O$ core, ∠CuOCu. The symmetric ($\nu_s$) and antisymmetric ($\nu_{as}$) stretch energies correlate with ∠CuOCu, and by fitting the four observables ($\nu_s$ and $\nu_{as}$ with $^{16}O_2$ and $^{18}O_2$) to NCA calculations, the observed stretches are consistent with a ∠CuOCu of 140° (Table S1). We further used these NCA calculations to evaluate the dependence of $\nu_s$ and $\nu_{as}$ of a $Cu_2O$ site on ∠CuOCu. As this angle decreases from 140° to 100°, the latter angle consistent with a bis-$\mu$-oxo dicopper structure, the predicted $\nu_s$ increases to 600 $cm^{-1}$ (Table S1). Thus, the observed

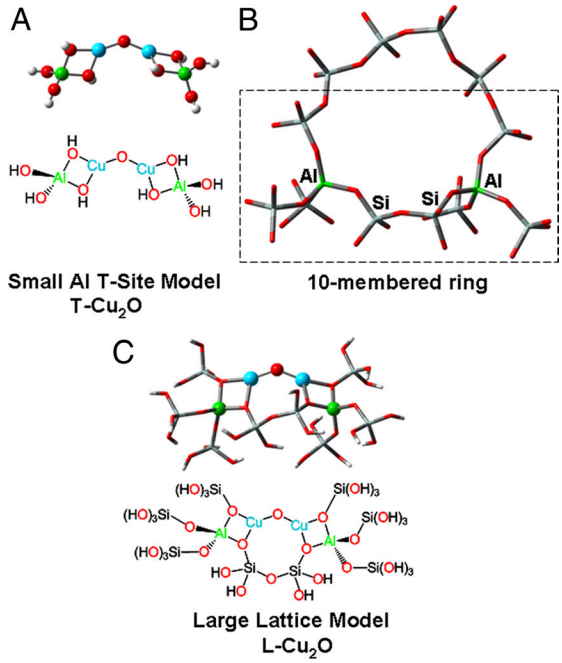


**Fig. 4.** Structural models of ZSM-5 and the $Cu_2O$ intermediate used for DFT calculations. (*A*) Small model, T—$Cu_2O$. (*B*) 10-membered ring of ZSM-5 containing two Al-sites separated by two Si-sites C. Large model constructed from part of a 10-membered ring (boxed atoms, B.), L-$Cu_2O$.

$\nu_s$ (≈600 $cm^{-1}$) in bis-$\mu$-oxo dicopper complexes is dominantly the result of the tight Cu—O—Cu angle associated with the presence of a second single atom bridge. The observed $\nu_s$ and $\nu_{as}$ for the active site of Cu-ZSM-5 require that this site has a wide ∠CuOCu (≈140°), and exclude the possibility of a second oxygen atom bridge.

Using the NCA-calculated ∠CuOCu of 140° as a starting point, these studies were expanded with DFT calculations to evaluate the capacity of the ZSM-5 lattice to host a $Cu_2O$ site. To form this active site, 4 electrons would have to be transferred to $O_2$ from $Cu^I$ ZSM-5, forming the $Cu_2O$ core and an additional oxo group. This can result in an active core containing either two $Cu^{III}$s or two $Cu^{II}$s with an accompanying 2-electron transfer from nearby $Cu^I$ ions to reduce the additional O atom.[‡] In ZSM-5, the 10-membered rings of the lattice are the only sites with pore-sizes appropriate for access of $O_2$, $N_2O$, and $CH_4$, and within these rings, a $Cu_2O$ core could only bind two lattice Os to each Cu (28). We therefore initially modeled the site with a tetrahedral $Al(OH)_4^-$ ligand (referred to as an Al T-site) bound bidentate to each Cu atom of the $Cu_2O$ core (Fig. 4*A*, small Al T-site model "T—$Cu_2O$" where the Hs cap the oxides in the Si lattice positions). This simplified ligation has been found to model the contribution of the lattice reasonably well (7). The wavefunction of T—$Cu^{III}{}_2O$ (singlet) is electronically unstable and relaxes to a T—$Cu^{II}{}_2O$ core with two additional holes delocalized to the T-site oxygens. A T—$Cu^{III}{}_2O$ can only be stabilized by adding a fourth ligand ($OH^-$) to each $Cu^{III}$. However, no feature associated with a Cu-OH stretch [computationally predicted at 655 $cm^{-1}$ ($\Delta(^{18}O_2)$ = 16 $cm^{-1}$)] is observed in the rR spectrum (Fig. 1). Thus, the experimental evidence argues against the presence of a fourth O-ligand that would be necessary to stabilize a $Cu^{III}{}_2O$ site. The calculations do, however, support a stable $Cu^{II}{}_2O$ electronic struc-

[‡]Electron transfer between molecules incorporated within a zeolite lattice has been observed for many redox pairs, and the zeolite lattice has been shown capable of facile charge transfer (27). The crystal structure of $Cu^I$-ZSM-5 shows 4 $Cu^I$ atoms within a 5Å distance of the two Cu atoms in the 10-membered ring, the predicted location of the $Cu_2O$ species (28).

**Table 2. Experimentally observed rR features, DFT vibrational predictions ($^{18}$O-isotopic shifts in parentheses) and DFT-optimized geometric parameters for the small Al T-site (T-Cu$^{II}_2$O) and large lattice (L-Cu$^{II}_2$O) models.**

| | rR Features | | | | Geometric Parameters | | |
|---|---|---|---|---|---|---|---|
| | Cu-O-Cu bend ($\Delta^{18}O_2$)/cm$^{-1}$ | $\nu_s$, ($\Delta^{18}O_2$)/cm$^{-1}$ | $\nu_{as}$, ($\Delta^{18}O_2$)/cm$^{-1}$ | Al-T-site, ($\Delta^{18}O_2$)/cm$^{-1}$ | ∠Cu-O-Cu | Cu-O, Å | Cu-Cu, Å |
| Experiment | 237 (−3) | 456 (−8) | 870 (−40) | 514/540 (0) | | | |
| T-Cu$^{II}_2$O (calcd) | 300 (−3) | 498 (−6) | 890 (−42) | 571 (0) | 138° | 1.74 | 3.29 |
| L-Cu$^{II}_2$O (calcd) | 253 (−2) | 456 (−5) | 852 (−37) | 556/568 (0) | 139° | 1.75/1.76 | 3.29 |

ture for the active site[§]. We evaluated the effect of the ∠CuOCu of the T—Cu$^{II}_2$O model on the DFT calculated $\nu_s$ and $\nu_{as}$ and found that, in agreement with the NCA calculations, an ∠CuOCu of 138° results in the best correlation with experimental data (Table 2, T—Cu$^{II}_2$O).

Within the 10-membered ring of ZSM-5, the experimentally calibrated NCA and DFT calculated structural parameters most closely fit an active site bound to two Al T-sites connected by two intermediate Si T-sites (Fig. 4*B*). This placement is also consistent with the crystal structure of Cu$^{I}$-ZSM-5, which resolves two Cu$^{I}$ atoms in the 10-membered ring separated by two intermediate T-sites (28). Thus, a larger model was formed with each Al T-site ligand extended with covalently bonded Si T-sites (Fig. 4*C*, Large Lattice Model, "L-Cu$_2$O"). The L-Cu$^{III}_2$O also electronically relaxes to a Cu$^{II}_2$O core upon optimization, confirming that the ZSM-5 lattice can only stabilize a Cu$^{II}_2$O core[¶]. The calculated ∠CuOCu is 139° with no constraints imposed on this core. The calculated $\nu_s$ (456 cm$^{-1}$) and $\nu_{as}$ (852 cm$^{-1}$) and $^{18}$O-isotopic shifts (5 and 37 cm$^{-1}$ respectively) for L-Cu$^{II}_2$O agree well with the experimentally observed values for these vibrations [$\nu_s$ = 456 cm$^{-1}$ ($\Delta(^{18}O_2)$ = 8 cm$^{-1}$) and $\nu_{as}$ = 870 cm$^{-1}$ ($\Delta(^{18}O_2)$ = 40 cm$^{-1}$)] (Table 2). Further, L-Cu$^{II}_2$O has calculated Al-T-site vibrations between 556 and 568 cm$^{-1}$, consistent with the observed $^{18}$O-isotope insensitive vibrations at 514 cm$^{-1}$ and 540 cm$^{-1}$ in Fig. 1. The Cu—O—Cu bending mode of L-Cu$^{II}_2$O is calculated at 253 cm$^{-1}$ ($\Delta(^{18}O_2)$ = 2 cm$^{-1}$), in agreement with the observed weak vibration at 237 cm$^{-1}$ ($\Delta(^{18}O_2)$ = 3 cm$^{-1}$) in Fig. 1.[‖] To investigate the origin of the absorption feature at 22,700 cm$^{-1}$, time dependent DFT calculations (TD-DFT) were performed on L-Cu$^{II}_2$O. These predict a single dominant feature at 23,400 cm$^{-1}$ originating from the bridging oxo ligand to Cu$^{II}$ charge transfer (Fig. S4), providing an assignment for the 22,700 cm$^{-1}$ band in Fig. 1 *Inset* A. The DFT calculations on L-Cu$^{II}_2$O thus accurately reproduce both the observed rR vibrations and the dominant absorption feature of oxygen-activated Cu-ZSM-5, a further confirmation of this geometric and electronic structural assignment.

**Reaction with CH$_4$.** The disappearance of the 22,700 cm$^{-1}$ absorption band as a function of temperature was used to evaluate the activation energy ($E_a$) for the reaction of oxygen-activated Cu-ZSM-5 with CH$_4$ (Fig. 5*A*). From the Arrhenius plots of the reaction at temperatures between 110 and 200 °C, the activation energy is 15.7 ± 0.5 kcal/mol (Fig. 5*C*, open square). This reaction has a kinetic isotope effect (KIE) (3.1 at 175 °C) resulting in an increase in the $E_a$ of the reaction by 3.1 ± 0.5 kcal/mol, obtained from an Arrhenius plot of the reaction with C$^2$H$_4$ (Fig. 5 *B* and *C*, filled triangle). This indicates that C—H bond breaking is involved in the rate limiting step of the oxidation of CH$_4$. Product analysis (by $^1$H-NMR, Fig. S5*A*) of the reaction of oxygen-activated Cu-ZSM-5 with CH$_2^2$H$_2$ confirms this KIE. Analysis of the KIE as a function of reaction temperature shows a similar increase in $E_a$ (2.1 ± 0.3 kcal/mol) for reaction with a C—$^2$H as compared with a C—H bond (Fig. S5*B*). Because comparable increases in $E_a$ are observed by monitoring the decay of the 22,700 cm$^{-1}$ band and by product analysis, the absorption feature can be directly correlated to the reactive site.

DFT calculations were used to obtain a transition state structure and evaluate the reactivity of the spectroscopically-validated L-Cu$^{II}_2$O model with CH$_4$ (Fig. 6*A*). The H atom abstraction reaction is calculated to have a zero-point corrected activation energy of 18.5 kcal/mol and an increase $E_a$ upon reaction with C$^2$H$_4$ of 1.3 kcal/mol, both in reasonable agreement with the experimentally observed $E_a$ of 15.7 kcal/mol and $\Delta E_a$ of 3.1 kcal/mol. The calculated H atom abstraction is endothermic by only 13.8 kcal/mol (ΔE), reflecting the difference in bond dissociation energy of H-CH$_3$ compared with that of the [Cu—OH—Cu]$^{2+}$ intermediate that would be generated. The strong O—H bond of the [Cu—OH—Cu]$^{2+}$ species (calculated bond dissociation energy of 90 kcal/mol) helps drive the reaction. The [Cu—OH—Cu]$^{2+}$ intermediate is best described as a delocalized-radical species, with Mulliken atomic spin densities of 0.26 and 0.44 on the Cu atoms and 0.17 on the bridging O. In the subsequent step, rebound of the hydroxyl radical (leaving 2 Cu$^{I}$) to couple with the methyl radical completes the reaction. Thus, the L-Cu$^{II}_2$O model of oxygen-activated Cu-ZSM-5 can abstract an H atom from CH$_4$ through a low activation barrier consistent with experiment (Fig. 6*A*).

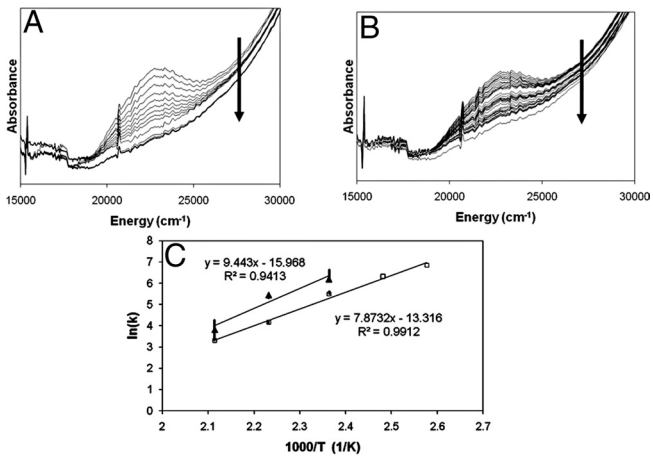


**Fig. 5.** $E_a$ and KIE measured from the decay of the 22,700 cm$^{-1}$ absorption band of O$_2$-activated Cu-ZSM-5 (Cu/Al = 0.54). (*A* and *B*) Decay of the 22,700 cm$^{-1}$ absorption band of an O$_2$ activated Cu-ZSM-5 (Cu/Al = 0.54) measured during reaction at 175 °C with CH$_4$ (*A*) and C$^2$H$_4$ (*B*). The arrow on the figures shows the evolution in time. Time interval between two spectra is 15 seconds. (*C*) Arrhenius' plots for CH$_4$ (open squares) and C$^2$H$_4$ (filled triangle).

[§]Calculations on T—Cu$^{II}_2$O predict a ferromagnetically coupled (triplet) ground state, 2 kcal/mol lower in energy than the antiferromagnetically coupled (singlet) state.

[¶]Calculations on the representative triplet state of L-Cu$^{II}_2$O are presented in the text as the singlet and triplet states of L-Cu$^{II}_2$O have nearly identical geometries and energies (within 0.5 kcal/mol) (Table S2 and Fig. S3).

[‖]While the Cu—Cu distance of L-Cu$^{II}_2$O (3.29Å) is inconsistent with the average Cu—Cu distance observed by EXAFS (2.87Å) (6), the active core is a minority species (5% of total Cu) and the Cu—Cu distance predicted from EXAFS is dominated by contributions of the majority, spectator Cu sites.

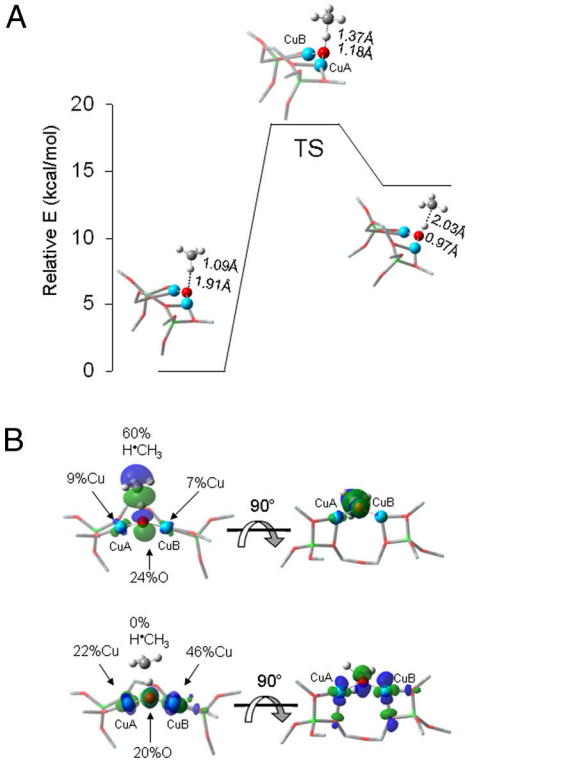


**Fig. 6.** DFT-calculated reactivity of L-$Cu^{II}_2O$ with $CH_4$. (*A*) Reaction coordinate of H atom abstraction from $CH_4$ by L-$Cu^{II}_2O$. (*B*) SOMOs at the TS shown with the line of $CH_4$ approach in the plane (*Left*) and below the plane of the figure (*Right*).

The electronic structure of L-$Cu^{II}_2O$ provides insight into the activation of $[Cu_2O]^{2+}$ for this reaction. There are two low-lying singly-occupied orbitals (SOMOs) that change along the reaction coordinate (Fig. 6*B*). Approaching the transition state, one of these orbitals, perpendicular to the Cu—O—Cu plane i.e., directed into the zeolite channel, localizes along the O—H—C vector and gains significant oxygen *p*-character (24% O with dominant delocalization into $H^{\bullet}CH_3$ in the transition state, Fig. 6*B*, *Upper*). The second singly-occupied low-lying molecular orbital is covalently delocalized between one of the coppers (CuA in Fig. 6*B*, *Lower*) (46%) and the oxygen atom (20%) with some delocalization into the second copper (CuB in Fig. 6*B*, *Lower*) (22%). This is essentially a $(CuB)^{II}$-$O^{\bullet-}$, cupric-oxyl species with some delocalization of the oxidized metal into the second Cu (CuA). This is further supported by changes in the Mayer bond order (29) (MBO) of the CuA—O and CuB—O bonds along the reaction coordinate. In L-$Cu^{II}_2O$, the MBO of the CuA—O bond is 1.24 and that of CuB—O is 1.02. The difference in the two MBOs is the direct result of constraints imposed by the zeolite lattice: The lattice oxygens form stronger bonds with CuB (MBOs of 0.54 and 0.44) than with CuA (MBOs of 0.46 and 0.37). The increased donation of the lattice Os to CuB leads to a decrease in the strength of the CuB—Oxo bond. At the transition state the CuA—O bond is significantly weaker than in the reactant L-$Cu^{II}_2O$ (MBO of 0.72, a decrease of 0.52). While the CuB—O bond also decreases in strength at the transition state (MBO of 0.86, a decrease of 0.19), this change is less than half that of the CuA—O bond. A cupric-oxyl species has been proposed as a highly activated intermediate in copper-oxygen chemistry, however, it has not been observed in any bioinorganic or model system (30). The significant oxygen p character in the low-lying half occupied orbital renders it highly activated as an acceptor orbital in H atom abstraction (Fig. 6*B Upper*).

## Conclusions

The oxygen-activated core of Cu-ZSM-5, reactive in the selective oxidation of methane into methanol, correlates to an absorption feature at 22,700 $cm^{-1}$. Raman vibrations of this active core are resonantly enhanced with $\lambda_{ex}$ within this absorption feature. $^{18}O$ isotope sensitive rR features profile this absorption feature, uniquely defining the active site structure. $^{18}O_2$ and $^{18,16}O_2$ labeling experiments exclude all previously defined oxygen bridged mononuclear and binuclear Cu sites for this active core. The energies, intensities, and isotope shifts of the observed vibrations lead to the assignment of this core as a mono-oxygen bridged binuclear Cu site. NCA and DFT calculations define the geometric and electronic structure of this core and provide insight into how the constrained lattice of ZSM-5 restricts the coordination environment of the bound Cu atoms and their spatial orientation resulting in the formation of a bent mono-$\mu$-oxo dicupric core. These calculations accurately reproduce the observed rR vibrations and isotope shifts and the dominant absorption feature.

The observation of a KIE (4.0 to 2.0 at 115–200 °C) shows C—H bond breaking is involved in the rate limiting step. Because similar increases in $E_a$ in C—H vs. C—$^2$H bond breaking were observed by monitoring the decay of the 22,700 $cm^{-1}$ band and by product analysis, the absorption feature can be directly correlated to the reactive site. DFT calculations show the formation of a $[Cu—OH—Cu]^{2+}$ intermediate with a calculated energy barrier in good agreement with experimental data. The strong O—H bond of the delocalized radical $[Cu—OH—Cu]^{2+}$ species helps drive the reaction. The electronic structure of L-$Cu^{II}_2O$ provides insight in the reaction mechanism and shows that upon approach of $CH_4$, one of the SOMOs of the $Cu_2O$ core gains significant oxygen *p*-character oriented into the zeolite channel and toward the H-$CH_3$ bond. At the transition state this results in the formation of a cupric-oxyl intermediate that is highly activated for H atom abstraction and explains the reactivity of the bent mono-$\mu$-oxo dicupric core in Cu-ZSM-5 in the selective oxidation of methane into methanol. While the nature of the active site in the enzyme particulate MMO is still a matter of discussion, our studies on Cu-ZSM-5 definitively determine that a binuclear cupric core can in fact perform the critical reaction of methane oxygenation.

## Materials and Methods

**Synthesis of Cu-ZSM-5 Samples.** A series of Cu-ZSM-5 samples with increasing Cu loading was prepared starting from Na-ZSM-5 (Si/Al = 12, ALSI-PENTA). Aqueous exchange of Na-ZSM-5 with $Cu(CH_3CO_2)_2 \cdot H_2O$ solutions of various $Cu^{2+}$ concentrations resulted in Cu-ZSM-5 with Cu/Al ratios of 0.10, 0.22, 0.31, 0.42 and 0.54, using procedures reported in ref. 5. The Cu and Al contents were determined by Inductively Coupled Plasma Atomic Absorption (ICP-AA).

**UV-Vis Spectra for Cu-ZSM-5 Samples After $O_2$, $N_2O$, He, $^{18}O_2$ Treatment.** In situ UV-vis-NIR spectra in the diffuse reflectance spectroscopy mode (DRS) of the Cu-ZSM-5 series were recorded on a Varian Cary 5 UV-vis-NIR spectrophotometer. All spectra were recorded at room temperature and cooling of the sample was done in an atmosphere of the corresponding treatment gas. $O_2$ and He treatments at 450 °C were done following procedures reported in ref. 5. The UV-vis spectra after interaction of a dehydrated Cu-ZSM-5 (Cu/Al = 0.54, dehydrated at 450 °C in He) with $N_2O$ and $O_2$ at temperatures <250 °C were recorded after the sample was flushed at room temperature with $O_2$ or $N_2O$ (5 min, 100vol.% $O_2$ or $N_2O$ flow of 50 mL·$min^{-1}$) and heated under this closed atmosphere (5 °C $min^{-1}$ to the indicated temperature).

For the $^{18}O$-labeled $O_2$ experiments ($^{18}O_2$ and a statistical mixture of $^{16}O_2$:$^{16/18}O_2$:$^{18}O_2$ with 1:2:1 ratio purchased from Buchem BV), a calcined Cu-ZSM-5 (Cu/Al = 0.54) was heated in He (heating rate of 1 °C $min^{-1}$ to 450 °C). At 450 °C a flow of 30 mL·$min^{-1}$ of the $^{18}O$-labeled $O_2$ (100 vol.%) was passed over the sample for 5 min. The sample was kept under a closed $^{18}O_2$ atmosphere at 450 °C for 30 min.

**Reaction with $CH_4$, $C^2H_4$ and $C^2H_2H_2$.** After $O_2$ calcination, the reactions with $CH_4$ and $C^2H_4$ (purchased from Aldrich) (total flow of 50 mL·$min^{-1}$, 10% $CH_4$ or $C^2H_4$ in He at reaction temperatures between 115 and 200 °C) were monitored. The setup consists of a plug-flow reactor (i.d. = 8 mm) fitted inside a furnace, a UV−Vis light source (Top Sensor Systems DH-2000 deuterium–halogen light

source) and a photodiode array detector (Ocean Optics SD 2000) connected to the catalyst bed via optical fiber technology (Top Sensor Systems FCB-UV400-ME cable and FCB-UV400G-0.1-XHT high-temperature probe) (6). Each spectrum is the result of the superposition of 300 scans in the 38,000–12,000 $cm^{-1}$ region, each taking 50 ms. Thus, one spectrum is obtained every 15 s.

For reaction with $C^2H_2H_2$ (purchased from Aldrich) and the subsequent extraction of deuterated methanol, an $O_2$ calcined Cu-ZSM-5 was reacted with $C^2H_2H_2$. After 2 min flow of 100% $C^2H_2H_2$ the sample was kept under a closed $C^2H_2H_2$ atmosphere for 20 min at the reaction temperature. The sample was then cooled to room temperature and the catalyst was poured into a screwtop vial containing 2 mL of $^2H_2O$. The closed vial was heavily stirred at room temperature for 20 h. The supernatant was sampled and transferred to an NMR tube for $^1$H-NMR analysis. $^1$H-NMR spectra were recorded on a Bruker (Fällanden, Switzerland) Avance II 500 spectrometer operating at 500.130 MHz. To quantitate the amount of methanol generated by low temperature $O_2$ and $N_2O$ activated Cu-ZSM-5, a dehydrated sample was activated in $O_2$ or $N_2O$ at 200 °C followed by reaction with $CH_4$ (10% in He, 50 mL·$min^{-1}$) at 200 °C. A known amount of acetonitrile was added to 1 mL of the supernatant as a calibrant and methanol concentration was determined by $^1$H-NMR.

**Resonance Raman Spectroscopy.** Resonance Raman spectra were recorded on a Princeton Instruments ST-135 back-illuminated CCD detector and on a Spex 1877 CP triple monochromator with 1,200, 1,800, and 2,400 grooves per millimeter of holographic spectrograph gratings. Excitation was provided by a Coherent I90C-K $Kr^+$ ion laser or an Innova Sabre 25/7 $Ar^+$ CW ion laser. The spectral resolution was $<2$ $cm^{-1}$. Spectra were recorded at room temperature at powers ranging from 5mW to 75mW at the sample. Sample preparation was the same as for the samples prepared for UV-vis measurements. Baseline spectra were collected using ground, activated charcoal in a quartz U-tube side arm.

**Calculations.** ***Normal coordinate analysis (NCA).*** Normal coordinate analysis (NCA) was based on a Urey-Bradley force field with the FG-matrix method of Wilson (31) and was performed on a triatomic Cu—O—Cu model ($C_{2v}$ symmetry) with a modified version of Schachtschneider's GMAT and FPERT programs (32, 33).
***DFT calculations.*** Spin-unrestricted DFT calculations were performed with Gaussian 03 (34) and the B3LYP functional. The 6–311G* basis set was used for the geometry optimizations and frequency calculations of T—$Cu_2O$. A split basis set was used for geometry optimizations, transition state searches, frequency calculations, and TD-DFT calculations of L-$Cu_2O$ with 6–311G* on the three Cu—O—Cu core atoms and the four Cu-coordinating lattice Os and 6–31G* on all other atoms. For reaction coordinate calculations, the split basis set included 6–311G* on the $CH_4$ atoms. Broken symmetry calculations were performed for all singlet spin states. Single point calculations were performed on optimized structures using the 6–311+G* basis set. For geometry optimizations and transition state searches with the L-$Cu_2O$ models, eight Si atoms were constrained at their crystallographically defined coordinates (35). Mulliken population analyses and MBO analyses were performed with QMForge (36) and vibrations and molecular orbitals were visualized in GaussView (37).

**ACKNOWLEDGMENTS.** This work was supported by the Institute for the Promotion of Innovation by Science and Technology in Flanders (IWT) (P.J.S.), K. U. Leuven graduate and postdoctoral fellowships (P.J.S.), Concerted Research Action (GOA), Long Term Structural Funding-Methusalem Funding by the Flemish Government (R.A.S. and B.F.S.), and National Institutes of Health Grant DK-31450 (to E.I.S.).

1. Rosenzweig AC, Frederick CA, Lippard SJ, Nordlund P (1993) Crystal-structure of a bacterial nonheme iron hydroxylase that catalyzes the biological oxid methane. *Nature* 366:537–543.
2. Lieberman RL, Rosenzweig AC (2005) Crystal structure of a membrane-bound metalloenzyme that catalyses the biological oxidation of methane. *Nature* 434:177–182.
3. Hakemian AS, Rosenzweig AC (2007) The biochemistry of methane oxidation. *Annu Rev Biochem* 76:223–241.
4. Himes RA, Karlin KD (2009) Copper-dioxygen complex mediated C—H bond oxygenation: Relevance for particulate methane monooxygenase (pMMO). *Curr Opin Chem Biol* 13:119–131.
5. Groothaert MH, Smeets PJ, Sels BF, Jacobs PA, Schoonheydt RA (2005) Selective oxidation of methane by the bis(mu-oxo)dicopper core stabilized on ZSM-5 and mordenite zeolites. *J Am Chem Soc* 127:1394–1395.
6. Groothaert MH, van Bokhoven JA, Battiston AA, Weckhuysen BM, Schoonheydt RA (2003) Bis(mu-oxo)dicopper in Cu-ZSM-5 and its role in the decomposition of NO: A combined in situ XAFS, UV-Vis-Near-IR, and kinetic study. *J Am Chem Soc* 125:7629–7640.
7. Goodman BR, Hass KC, Schneider WF, Adams JB (1999) Cluster model studies of oxygen-bridged Cu pairs in Cu-ZSM-5 catalysts. *J Phys Chem B* 103:10452–10460.
8. Yumura T, Takeuchi M, Kobayashi H, Kuroda Y (2009) Effects of ZSM-5 zeolite confinement on reaction intermediates during dioxygen activation by enclosed dicopper cations. *Inorg Chem* 48:508–517.
9. Smeets PJ, Groothaert MH, Schoonheydt RA (2005) Cu based zeolites: A UV-vis study of the active site in the selective methane oxidation at low temperatures. *Catal Today* 110:303–309.
10. Henson MJ, Mukherjee P, Root DE, Stack TDP, Solomon EI (1999) Spectroscopic and electronic structural studies of the Cu(III)(2) bis-mu-oxo core and its relation to the side-on peroxo-bridged dimer. *J Am Chem Soc* 121:10332–10345.
11. Mahapatra S, et al. (1995) A new intermediate in copper dioxygen chemistry—Breaking the O—O bond to form a $(Cu_2(\mu\text{-}O)_2)^{2+}$ Core. *J Am Chem Soc* 117:8865–8866.
12. Baldwin MJ, et al. (1992) Spectroscopic studies of side-on peroxide-bridged binuclear copper(II) model complexes of relevance to oxyhemocyanin and oxytyrosinase. *J Am Chem Soc* 114:10421–10431.
13. Maiti D, et al. (2007) A 1 : 1 copper-dioxygen adduct is an end-on bound superoxo copper(II) complex which undergoes oxygenation reactions with phenols. *J Am Chem Soc* 129:264–265.
14. Chen P, Root DE, Campochiaro C, Fujisawa K, Solomon EI (2003) Spectroscopic and electronic structure studies of the diamagnetic side-on Cu-II-superoxo complex Cu(O-2)[HB(3-R-5-(i)Prpz)(3)]: Antiferromagnetic coupling versus covalent delocalization. *J Am Chem Soc* 125:466–474.
15. Chen P, Fujisawa K, Solomon EI (2000) Spectroscopic and theoretical studies of mononuclear copper(II) alkyl- and hydroperoxo complexes: Electronic structure contributions to reactivity. *J Am Chem Soc* 122:10177–10193.
16. Baldwin MJ, et al. (1991) Spectroscopic and theoretical-studies of an end-on peroxide-bridged coupled binuclear copper(II) model complex of relevance to the active-sites in hemocyanin and tyrosinase. *J Am Chem Soc* 113:8671–8679.
17. Root DE, Mahroof-Tahir M, Karlin KD, Solomon EI (1998) Effect of protonation on peroxo-copper bonding: Spectroscopic and electronic structure study of [Cu-2((UN-O-)(OOH)](2+). *Inorg Chem* 37:4838–4848.
18. Pate JE, Cruse RW, Karlin KD, Solomon EI (1987) Vibrational, electronic, and resonance Raman spectral studies of $[Cu_2(XYL\text{-}O\text{-})O_2]^+$, a copper(II) peroxide model complex of oxyhemocyanin. *J Am Chem Soc* 109:2624–2630.
19. Thamann TJ, Loehr JS, Loehr TM (1977) Resonance Raman study of oxyhemocyanin with unsymmetrically labeled oxygen. *J Am Chem Soc* 99:4187–4189.
20. Czernuszewicz RS, Sheats JE, Spiro TG (1987) Resonance Raman-spectra and excitation profile for $[Fe_2O(O_2CCH_3)_2(Hb(Pz)_3)_2]$, a hemerythrin analog. *Inorg Chem* 26:2063–2067.
21. Wing RM, Callahan KP (1969) Characterization of metal-oxygen bridge systems. *Inorg Chem* 8:871–874.
22. Iwamoto M, et al. (1991) Removal of nitrogen monoxide through a novel catalytic process. 1. Decomposition on excessively copper-ion exchanged ZSM-5 zeolites. *J Phys Chem* 95:3727–3730.
23. Rice MJ, Chakraborty AK, Bell AT (2000) Theoretical studies of the coordination and stability of divalent cations in ZSM-5. *J Phys Chem B* 104:9987–9992.
24. Karlin KD, Gultneh Y, Hayes JC, Zubieta J (1984) Copper(I) dioxygen reactivity. Reaction of a 3-coordinate copper(I) complex with O-2, with evidence for a binuclear oxo copper(II) species—Structural characterization of a parallel-planar dihydroxo-bridged dimer. *Inorg Chem* 23:519–521.
25. Kitajima N, Koda T, Hashimoto S, Kitagawa T, Morooka Y (1991) Synthesis and characterization of the dinuclear copper(II) complexes $[Cu(HB(3,5\text{-}Me_2pz)_3)]_2X$ (X = $O^{2-}$, $(OH)_2^{2-}$, $CO_3^{2-}$, $O_2^{2-}$). *J Am Chem Soc* 113:5664–5671.
26. Obias HV, et al. (1998) Peroxo-, oxo-, and hydroxo-bridged dicopper complexes: Observation of exogenous hydrocarbon substrate oxidation. *J Am Chem Soc* 120:12960–12961.
27. Yoon KB (1993) Electron-transfer and charge-transfer reactions within zeolites. *Chem Rev* 93:321–339.
28. Mentzen BF, Bergeret G (2007) Crystallographic determination of the positions of the copper cations in zeolite MFI. *J Phys Chem C* 111:12512–12516.
29. Mayer I (1983) Charge, bond order and valence in the abinitio Scf theory. *Chem Phys Lett* 97:270–274.
30. Decker A, Solomon EI (2005) Dioxygen activation by copper, heme and non-heme iron enzymes: Comparison of electronic structures and reactivities. *Curr Opin Chem Biol* 9:152–163.
31. Wilson EB, Decius JC, Cross PC (1980) *Molecular Vibrations* (Dover, New York, NY).
32. Schachtschneider JH (1964) Tech. Rep. Nos. 231–264 and 57–65 (Shell Development Co., Emeryville, CA).
33. Fuhrer H, Kartha VB, Kidd KG, Krueger PJ, Mantsch HH (1976) *NRCC Bulletin No. 15* (National Research Council, Ottowa, ON).
34. Frisch MJ, et al. (2003) Gaussian 03, Revision C. 02 (Gaussian, Inc., Wallingford, CT).
35. Olson DH, Kokotailo GT, Lawton SL, Meier WM (1981) Crystal-structure and structure-related properties of ZSM-5. *J Phys Chem* 85:2238–2243.
36. Tenderholt AL (2007) QMForge, Version 2.1 (Stanford University, Stanford, CA).
37. Dennington IIR, et al. (2003) GaussView, Version 3.09 (Semichem, Inc., Shawnee Mission, KS).